Electronic Supplementary Material (ESI) for Nanoscale.
This journal is © The Royal Society of Chemistry 2016

# Electronic Supplementary Information

# Low-Coordinated Surface Atoms of CuPt Alloy Cocatalysts on $TiO_2$ for Enhanced Photocatalytic Conversion of $CO_2$

*Sooho Lee,[a] Sunil Jeong,[a] Whi Dong Kim,[a] Seokwon Lee,[a] Kangha Lee,[a] Wan Ki Bae,[b] Jun Hyuk Moon,[c] Sangheon Lee*[d] and Doh C. Lee*[a]*

[a]Department of Chemical and Biomolecular Engineering (BK21+ Program), KAIST Institute for the Nanocentury, Korea Advanced Institute of Science and Technology (KAIST), Daejeon 34141, Korea

[b]Photo-Electronic Hybrids Research Center, Korea Institute of Science and Technology (KIST), 14-gil 5, Hwarang ro, Seongbuk-gu, Seoul 136-791, Korea

[c]Department of Chemical Biomolecular Engineering, Sogang University, Seoul 04107, Korea

[d]Department of Chemical Engineering and Materials Science, Ewha Womans University, Seoul 03760, Korea

## Experimental

### Synthesis of CuPt–$TiO_2$

CuPt-$TiO_2$ photocatalysts were prepared via previously reported procedures.[S1] 7.2 mg of copper nitrate trihydrate (99-104%, Aldrich), 5.4 mg of chloroplatinic acid hydrate (>99.9%, Aldrich), and 1.0 g of $TiO_2$ nanoparticles (P25, Degussa) were mixed in 10 mL of deionized (DI) water for 30 min for the case of obtain 1.2 nm CuPt–$TiO_2$. For synthesis of 2.3 nm, 3.6 nm and 4.6 nm CuPt–$TiO_2$, 36 mg, 72 mg and 144 mg of copper nitrate trihydrate and 27 mg, 54 mg and 108 mg of chloroplatinic acid hydrate were mixed with $TiO_2$ in 10 mL of DI water, respectively. The mixture was then heated for 10 h at 373 K to obtain $TiO_2$ powder evenly mixed with Cu and Pt precursors. The dried powder was calcined for 2 h at 673 K under air in a tube furnace. The ramping rate was 2 K/min. Then, the resultant powder was placed under $H_2$ flow for 2 h at 673 K.

### Photocatalytic $CO_2$ conversion

Photocatalytic, heterogeneous catalytic reduction of $CO_2$ was conducted in a reaction chamber with a total volume of 70 mL. Before the reaction, a film with an area of 1.0 $cm^2$ was prepared by drop-casting 0.4 mg of CuPt–$TiO_2$ in 100 $\mu$L of ethanol for photocatalytic $CO_2$ conversion and was placed vertically in a reaction chamber. The quartz plate with photocatalyst film was placed at the center of a reaction chamber. 50 $\mu$L of water was added into a reaction chamber, and then the reaction chamber was purged with $CO_2$ gas for 30 min. A 150 W Xe lamp (ABET Technologies 10500)

was used as a light source. Temperature and pressure of the reactor were kept at 313 K and 1.2 atm, respectively. 0.25 mL of gas was taken from the reactor with a syringe every hour and its composition was analyzed using gas chromatography (GC, YL6500) equipped with a thermal conductivity detector (TCD) and a flame ionization detector (FID).

**Characterization**

Transmission electron microscopy (TEM, Philips Tecnai F30 (300 kV)) and high-angle annular dark field (HAADF) scanning transmission electron microscopy (STEM) (FEI Titan Cubed G2 60-300 (200kV)) were employed to analyze the morphology of CuPt–$TiO_2$. X-ray and ultraviolet photoelectron spectroscopy (XPS and UPS, Sigma Probe) were used to examine alloy formation and reaction mechanism. Fourier-transform infrared (FT-IR) spectra were collected using an FT-IR spectrometer (Alpha FT-IR, Bruker). In addition, an inductively coupled plasma mass spectrometer (ICP-MS) was used to analyze the ratio of Cu to Pt (Agilent ICP-MS 7700S).

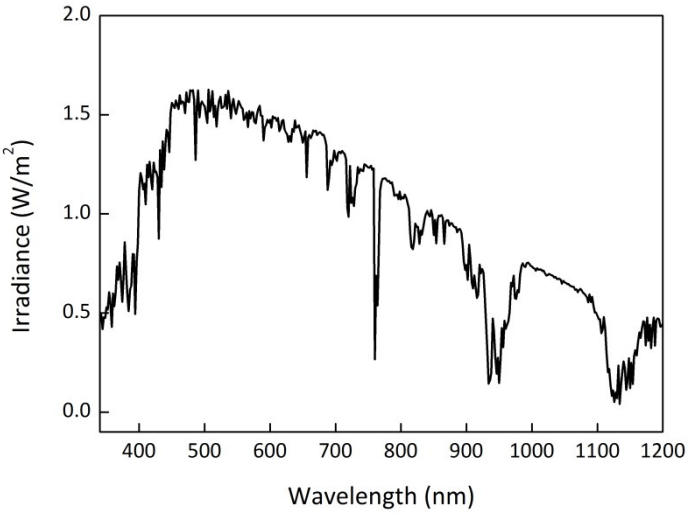


**Fig. S1** Spectrum of 150 W Xe lamp used for photocatalytic $CO_2$ conversion.

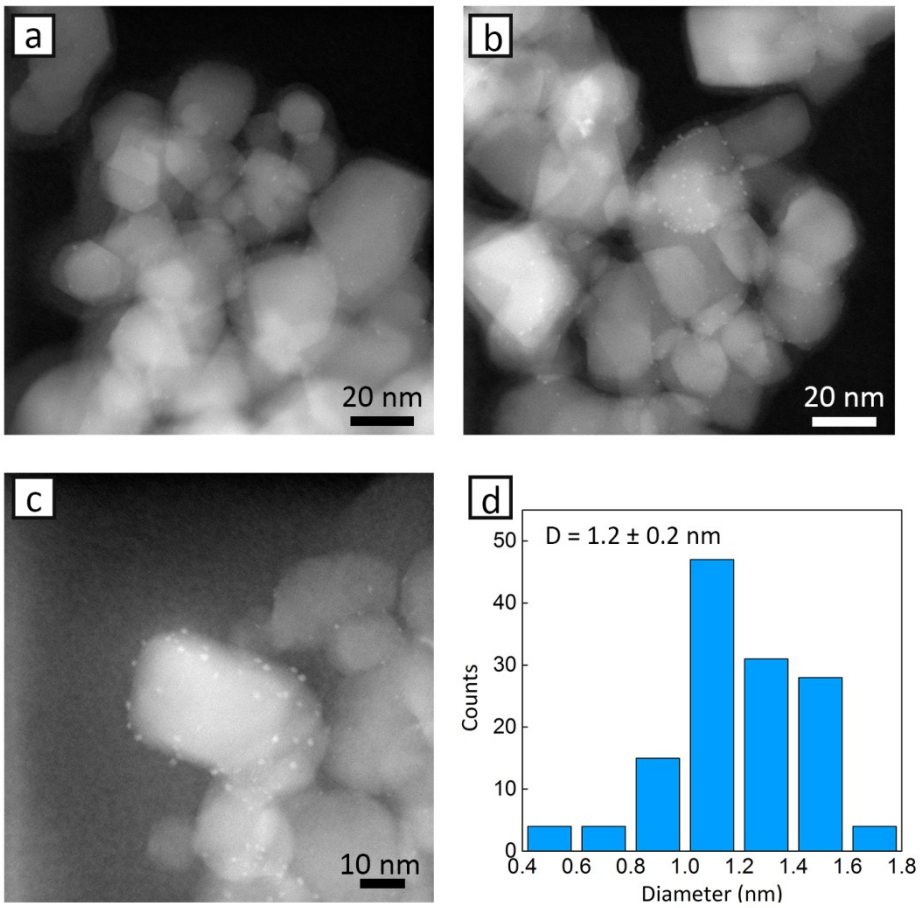


**Fig. S2** (a-c) TEM images and (d) size distribution of 1.2 nm CuPt–$TiO_2$.

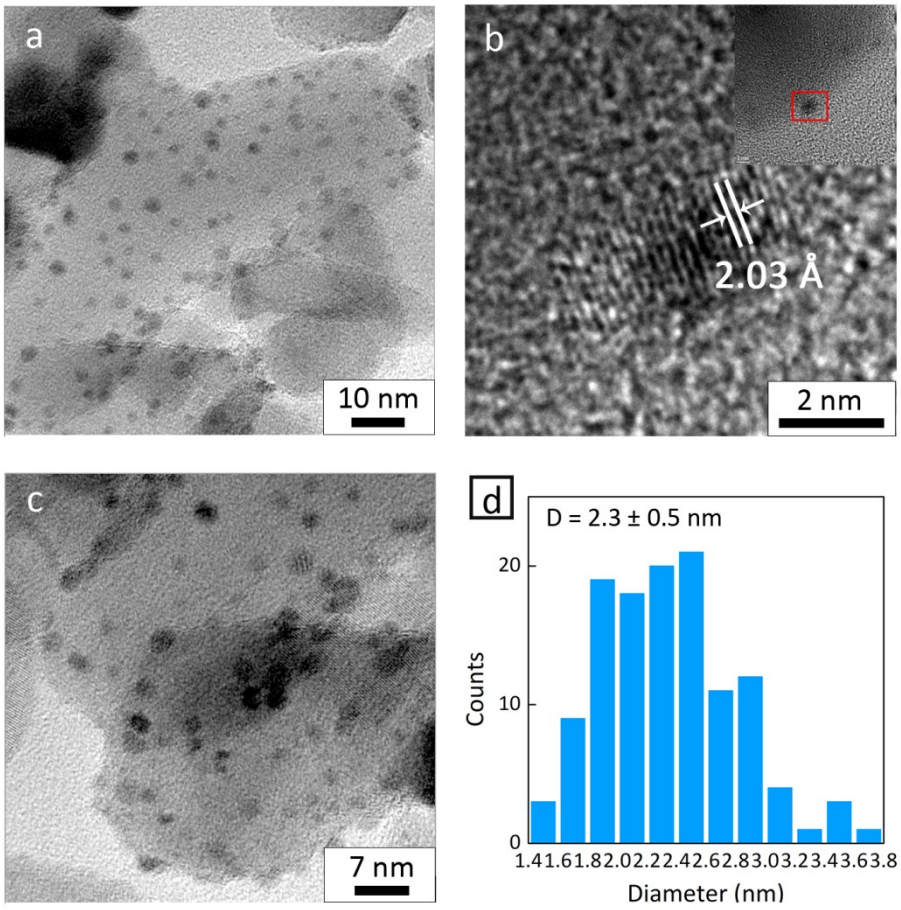


**Fig. S3** (a-c) TEM images and (d) size distribution of 2.3 nm CuPt–$TiO_2$. The d-spacing of CuPt(100) in (b) is between standard Cu(100) ((JCPDS 04-0836, 0.904 Å) and Pt(100) (JCPDS 04-0802, 3.92 Å).

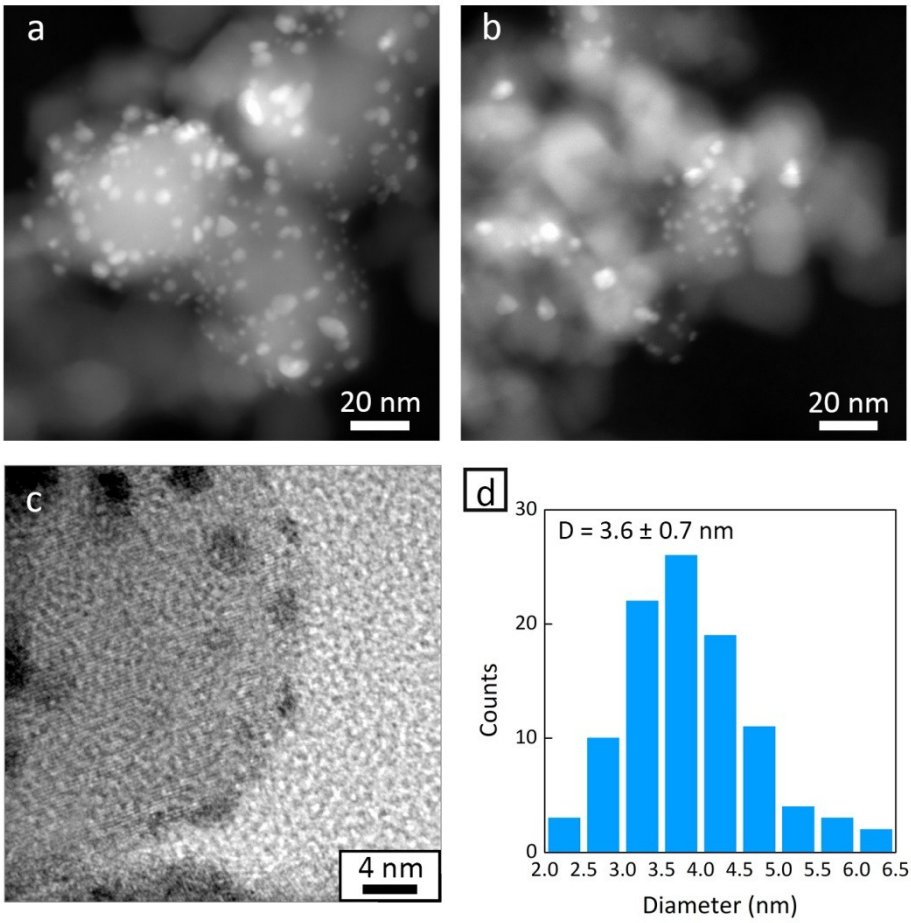


**Fig. S4** (a-c) TEM images and (d) size distribution of 3.6 nm CuPt–$TiO_2$.

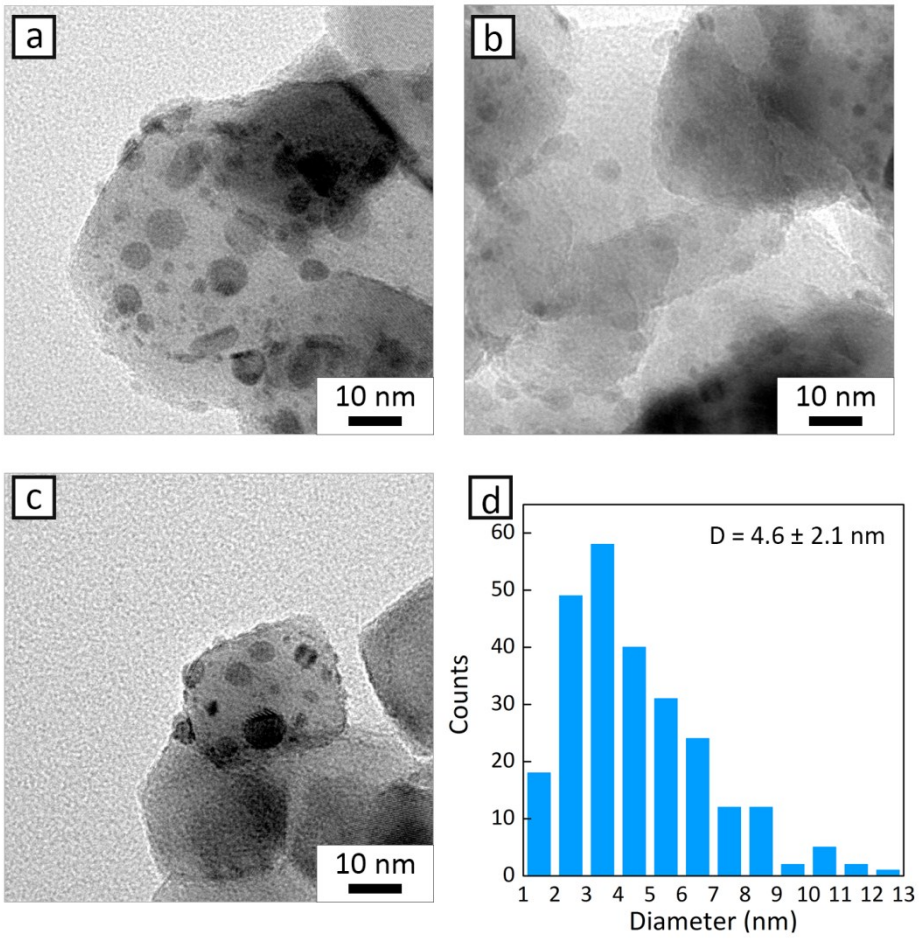


**Fig. S5** (a-c) TEM images and (d) size distribution of 4.6 nm CuPt–$TiO_2$.

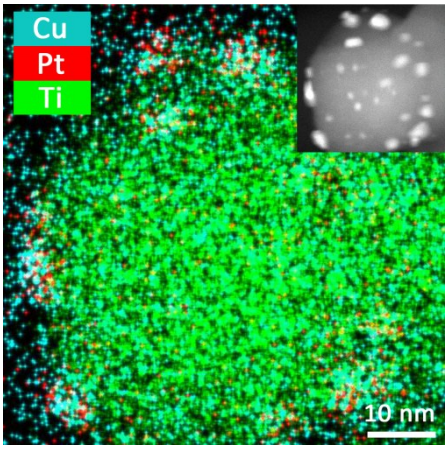


**Fig. S6** Overlayered elemental mapping image of CuPt–$TiO_2$: blue, red, and green dots represent Cu, Pt, and Ti, respectively.

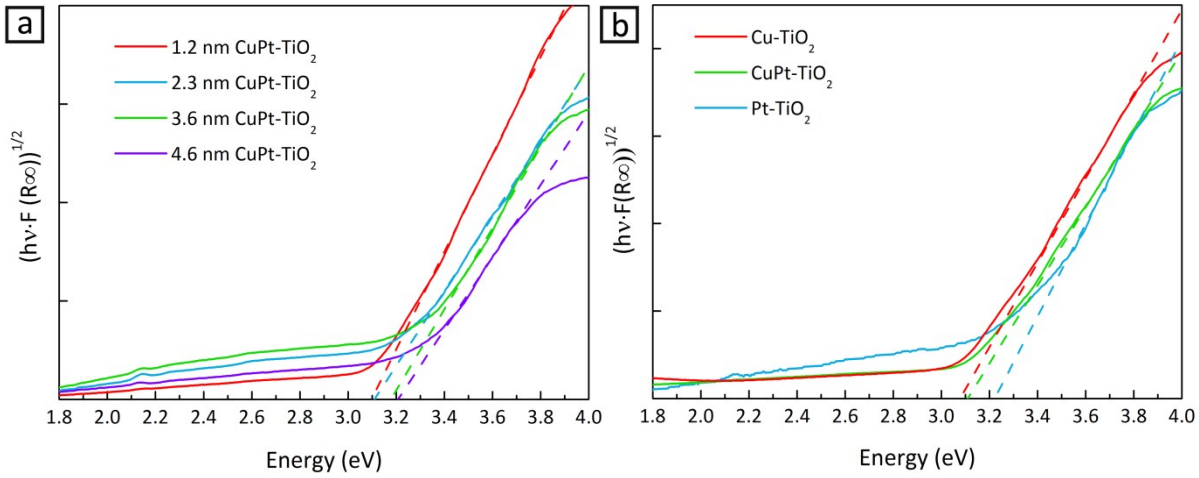


**Fig. S7** Transformed Kubelka-Munk functions of (a) 4 sizes of CuPt–$TiO_2$ and (b) Cu, Pt, and CuPt cocatalysts deposited on $TiO_2$.

**Table S1** Absorption onset of photocatalysts estimated from Tauc plot

| Size | 1.2 nm CuPt–$TiO_2$ | 2.3 nm CuPt–$TiO_2$ | 3.6 nm CuPt–$TiO_2$ | 4.6 nm CuPt–$TiO_2$ |
|---|---|---|---|---|
| Bandgap (eV) | 3.10 | 3.11 | 3.17 | 3.20 |

| Metal | Cu-$TiO_2$ | Pt-$TiO_2$ | CuPt-$TiO_2$ |
|---|---|---|---|
| Bandgap (eV) | 3.09 | 3.23 | 3.10 |

**Computational Details**

Surfaces of Cu and bimetallic CuPt alloy are modeled as face-centered-cubic (FCC) (111)/(211) slabs containing four layers of 2×2/1×2 hexagonal/cubic supercell, each of which contains four/six atoms. The flat (111) surfaces represent the highest-coordinated catalytic surfaces, whereas the stepped (211) surfaces include the effect of low-coordinated surface sites such as edges and corners. As a result, the bimetallic CuPt(211) surface can be represented by the two different model surfaces, each denoted as CuPt(211)-A and CuPt(211)-B, while the bimetallic CuPt(111) surface can be represented by the single model surface, denoted as CuPt(111). Note that the CuPt(211)-A surface includes Pt atoms at the edge, while the edge of the CuPt(211)-B consists only of Cu atoms.

The calculations reported herein were performed on the basis of spin polarized density functional theory (DFT) within the revised Perdew-Burke-Ernzerhof (rPBE) functional, as implemented in the Vienna Ab-initio Simulation Package (VASP).[S2] The projector augmented wave (PAW) method with a planewave basis set was employed to describe the interaction between ion cores and valence electrons.[S3] An energy cutoff of 350 eV was applied for expansion of the electronic eigenfunctions. For the supercell, each model surface is separated from its periodic images in the vertical direction by a vacuum space corresponding to seven atomic layers. While the bottom two layers of the five-layered slab are fixed at corresponding bulk positions, the upper two layers are fully relaxed using the conjugate gradient method until residual forces on all the constituent atoms become smaller than $5\times10^{-2}$ eV/A. For the Brillouin zone integration of (111)/(211) surfaces,[S4] we used a (6×6×1)/(4×6×1) Monkhorst-Pack mesh of k points to determine the optimal geometries and total energies of systems.

The $CO_2$ reduction process in this work can be viewed as transfer of a series of proton-electron ($H^+ + e^-$) pairs to the adsorbed intermediates on the catalyst surface, along with adsorption of reactants and desorption of products. To evaluate the catalytic activity of a given surface, it is essential to calculate the relative free energy ($\Delta G$) of each intermediate state to that of $CO_2(g)$. As an example, for an intermediate state $*CO_2H_n$ [the asterisk (*) indicates that the species is adsorbed on the surface], to which $CO_2(g)$ is reduced by taking $n(H^+ + e^-)$, the relative free energy [$\Delta G$] of $*CO_2H_n$ is given by

$$\Delta G = G(*CO_2H_n) - \mu(CO_2(g)) - n[\mu(H^+) + \mu(e^-)], \quad \text{(EQ01)}$$

where G(M) is the free energy of the state M, $n$ is the number of proton-electron pairs transferred relative to $CO_2$, $e$ is the elementary (positive) charge, and $\mu$(M) is the chemical potential of M. Chemical potentials of a solvated proton [$\mu(H^+)$] and an electron [$\mu(e^-)$] are treated by the computational chemical electrode (CHE) model,[S5,S6] where $\mu(H^+)$ is equal to half of the chemical potential of gaseous hydrogen [$0.5\mu(H_2)$] and $\mu(e^-)$ corresponds to $-eU$, where $U$ is the applied bias. As a result, equation EQ01 can be rewritten as

$$\Delta G = G(*CO_2H_n) - \mu(CO_2(g)) - n[0.5\mu(H_2(g)) - eU]. \quad \text{(EQ02)}$$

For adsorbed species, electronic energies (E) are converted into free energies (G) by including zero-point energies and entropies, which are calculated by performing the harmonic normal-mode analysis based on the standard method.[S7] The vibrational frequencies, which are needed for the harmonic normal-mode analysis, are calculated for the Cu(111) and Cu(211) surfaces and assumed to be constant for all (111) and (211) alloy surfaces, respectively. This approximation has been justified because the vibrations in zero-point energy and entropic contribution were small, compared to the variation in electronic energy.[S8,S9] For non-adsorbed species, electronic energies (E) were converted into chemical

potentials (μ) at 18.5 °C by standard ideal-gas methods.[S7] The chemical potentials of $H_2$(g), CO(g), and $CO_2$(g) are calculated at 101325 Pa (1 atm), and the chemical potential of water vapor is adjusted to a pressure of 3534 Pa, which is the vapor pressure of water (at which point the chemical potential of liquid and vapor phases are equal).[S6] Finally, the RPBE gas-phase correction of +0.45 eV is applied to $CO_2$(g).[S6]

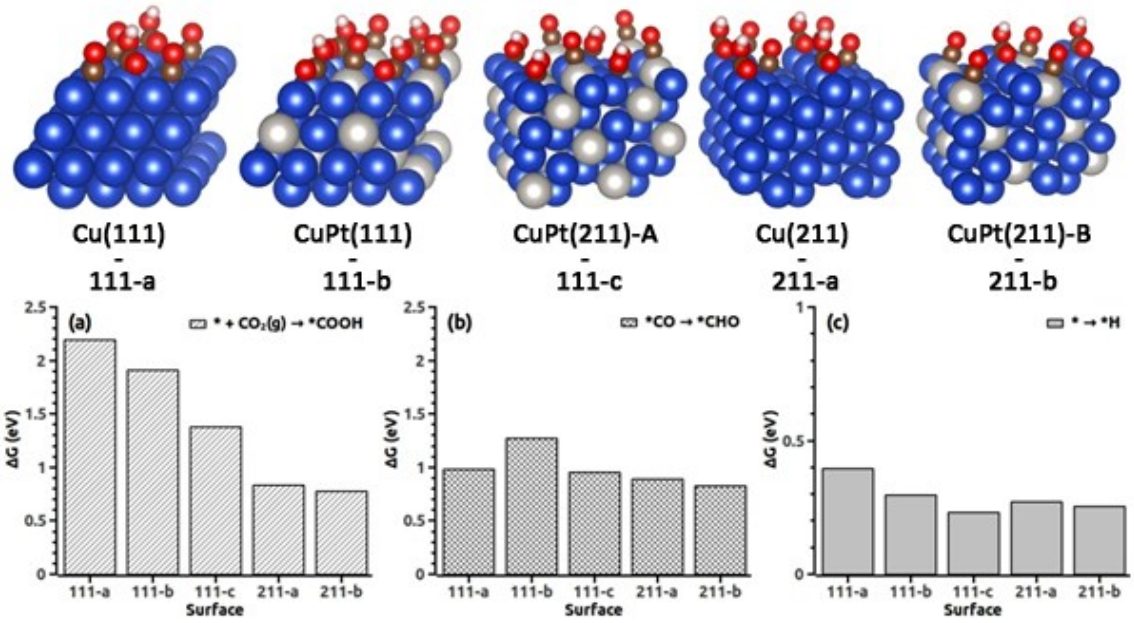


**Fig. S8** Calculated thermodynamic free energy barriers for (a) * + $CO_2$(g) $\overset{(H^+ + e^-)}{\rightarrow}$ *COOH, (b) *CO + $H_2O$(g) $\overset{(H^+ + e^-)}{\rightarrow}$ *CHO + $H_2O$(g), and (c) * $\overset{(H^+ + e^-)}{\rightarrow}$ *H steps over the five CO-covered surfaces. The inset shows geometric structure of the COOH adsorbed on the CO-covered surfaces. Blue, gray, brown, red, and white spheres denote Cu, Pt, C, O, and H atoms, respectively.

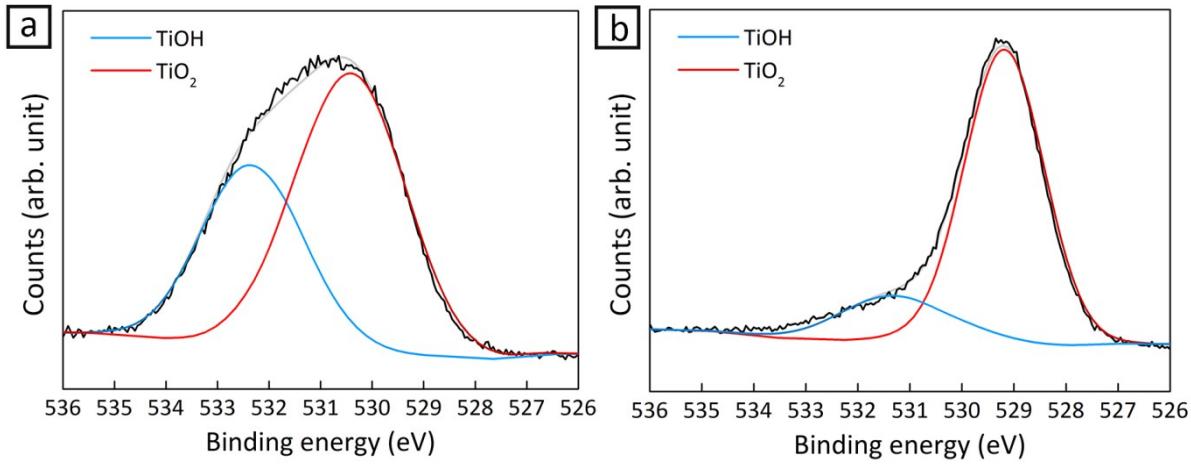


**Fig. S9** XPS spectra of 3.6 nm CuPt–$TiO_2$ (a) before and (b) after photocatalytic reaction.

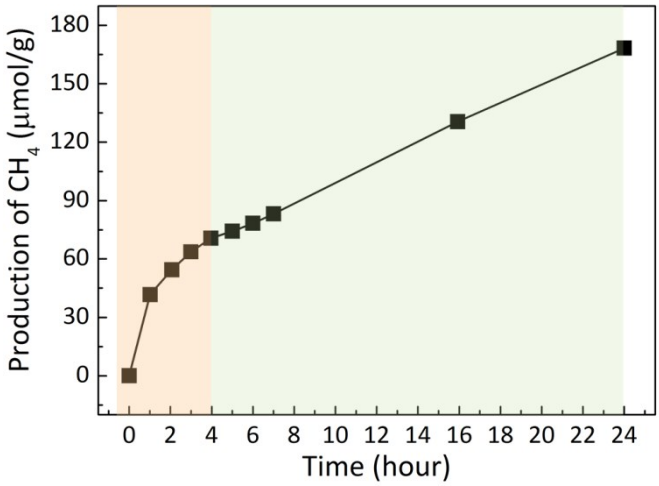


**Fig. S10** Photocatalytic $CO_2$ reduction using 1.2 nm CuPt–$TiO_2$ for 24 h. CuPt with hydroxyl group contributes to $CH_4$ production for first 4 h (orange region) whereas CuPt–$TiO_2$ without hydroxyl group forms $CH_4$ after consumption of TiOH (green region). The production rate of $CH_4$ decreased from 11.3 to 4.5 μmol/g·hr after TiOH appears to dissipate at about 4 h.

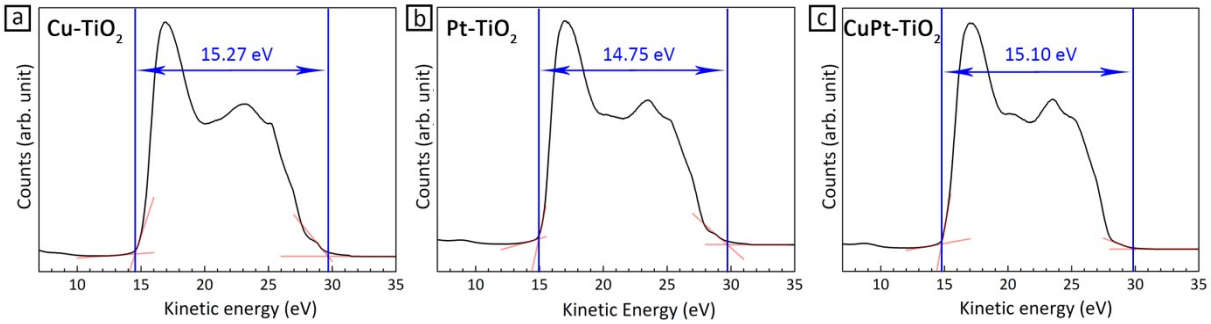


**Fig. S11** UPS spectra of (a) Cu–, (b) Pt–, and (c) CuPt–$TiO_2$. Work functions are determined by subtracting the difference between the secondary electron cutoff and Fermi energy level from excitation beam (21.2 eV).

**Table S2** Comparison of Pt/Cu ratio from experimental and ICP-MS

| | Experimental | ICP-MS |
|---|---|---|
| Pt/Cu ratio (mol/mol) | 0.67 | 0.60 |

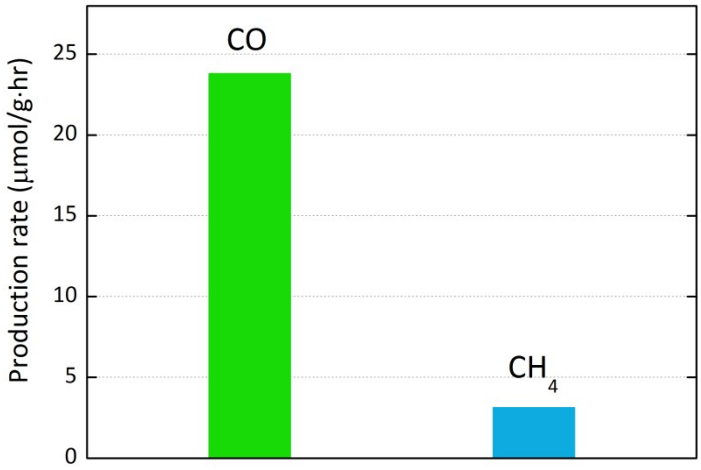


**Fig. S12** Photocatalytic production of CO and $CH_4$ via reduction of $CO_2$ using Cu–$TiO_2$ as a photocatalyst.

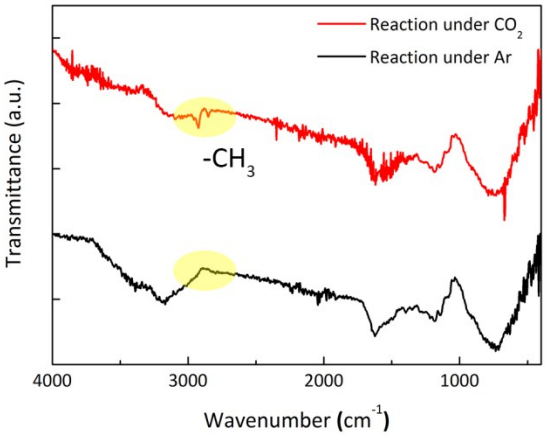


**Fig. S13** FT-IR spectra of 1.2 nm CuPt–$TiO_2$ illuminated under $CO_2$ (red line), and under Ar (black line) for 4 h.

**References**

S1. Y. Shiraishi, H. Sakamoto, Y. Sugano, S. Ichikawa and T. Hirai, *ACS Nano*, 2013, **7**, 9287-9297.

S2. Kresse, G.; Furthmuller, J., *VASP the Guide, Vienna University of Technology: Vienna, Austria* **2001**.

S3. Blochl, P. E., Projector Augmented-Wave Method. *Phys. Rev. B* **1994,** *50* (24), 17953-17979.

S4. Blochl, P. E.; Jepsen, O.; Andersen, O. K., Improved Tetrahedron Method for Brillouin-Zone Integrations. *Phys Rev B* **1994,** *49* (23), 16223-16233.

S5. Nørskov, J.K.; Rossmeisl, J.; Logadottir, A.; Lindqvist, L.; Kitchin, J.R.; Bligaard, T.; Jonsson, H., *J. Phys. Chem. B.* **2004**, 108, 17886.

S6. Peterson, A.A.; Abild-Pedersen, F.; Studt, F.; Rossmeisl, J; Nørskov, J.K., *Energy Environ. Sci.* **2010**, 3, 1311-1315.

S7. Cramer, C.J. Essentials of Computational Chemistry (Wiley, 2004), 2nd edn.

S8. Jones, G.; Jakobsen, J.G.; Shim, S.S.; Kleis, J.; Andersson, M.P.; Rossmeisl, J.; Abild-Pedersen, F.; Bligaard, T.; Helveg, S.; Hinnemann, B.; Rostrup-Nielsen, J.R.; Chorkendorff, I.; Sehested, J.; Nørskov, J.K. *J. Catal.* **2008**, 259, 147-160.

S9. Yoo, J.S.; Abild-Pedersen, F.; Nørskov, J.K.; Studt, F, *ACS Catal.* **2014**, 4, 1226-1233.